# THERMO-HYDRAULIC ANALYSIS OF THE PBMR USED FUEL TANK USING COMPUTATIONAL FLUID DYNAMICS

**Carel Frederik Viljoen**

**B.Eng. (Mechanical)**

**Mini-dissertation submitted in partial fulfilment of the requirements for the degree**

**Magister Ingeneriae (Mechanical Engineering)**

**School of Mechanical and Materials Engineering**

**at the**

**Potchefstroomse Universiteit vir Christelike Hoër Onderwys**

**Promoter: Prof. CG du Toit**

**Assistant Promotor: Dr. M Kleingeld**

**Potchefstroom**

**2003**

**Abstract**

The Pebble Bed Modular Reactor (PBMR) is a 4th generation nuclear reactor based on the HTR-Modul of Siemens currently being developed by Eskom in South Africa. The major safety characteristics of the PBMR are the fuel design and physical dimensions that make it an inherently safe reactor. This means that the reactor will not melt down like a typical Light Water Reactor (LWR) when cooling of the reactor is lost.

The thermo-hydraulic analysis of the Used Fuel Tank (UFT) is of great importance in the safety analysis of the PBMR. The UFT is one of two types of tanks that will be used to store fuel that has been in the reactor for a finite time. The fuel would therefore contain fission products and would generate decay heat. This decay heat should be removed to limit the temperature of the fuel.

The temperature of the fuel should be limited to prevent the release of fission products to the environment. The temperature limit on the fuel during storage is required to ensure that the graphite in the fuel does not oxidize in the presence of oxygen. The fuel is normally kept in a helium environment, but it must be shown that the fuel is safe when there is air ingress into the system.

The purpose of this study is therefore to determine the temperature distribution in the fuel and the components of the used fuel tank for different scenarios. This includes the forced cooling of the tanks and the possibility of cooling the tanks with natural convection.

Computational Fluid Dynamics (CFD) was used to model the various heat transfer mechanisms present. This includes convection heat transfer between the gases and the solids, conduction through the solids and thermal radiation between most of the surfaces. The effect of natural convection was also included, as the pipes through the tank cause result in high mass flow through these pipes due to the buoyancy effect.

The results show that the fuel temperature will not exceed the allowable limit during forced cooling if the Heating, Ventilation and Air-conditioning (HVAC) is

supplied at 6 kg/s. The possibility of cooling the tanks with passive means during upset events looks promising, but it is dependant on the design of the chimneys. The chimney cross-flow area was the most significant factor influencing the air mass flow through the system.

The chimney design and the rest of the system not included in this study should be analysed in detail before the passive operation of the system can be guaranteed.

# Uittreksel

Die Korrelbed Modulêre Reaktor, wat deur Eskom in Suid-Afrika onwikkel word, is 'n vierde generasie kern reaktor gebaseer op die HTR-Modul van Siemens. Die belangrikste veiligheidskarakteristieke van die die reaktor is die brandstof ontwerp en die fisiese dimensies van die reaktor wat die reaktor inherent veilig maak. Dit beteken dat die reaktor nie soos 'n gewone Ligte Water Reaktor (LWR) sal smelt indien die verkoeling sou faal nie.

Die termo-hidrouliese analise van die brandstof stoortenk is van belang in die veiligheidsanalise van die PBMR. Die tenk is een van twee tipes wat gebruik gaan word om brandstof te stoor wat vir 'n beperkte tyd in die reaktor was. Die brandstof bevat dus klowingsprodukte wat radioaktief verval. Die hitte wat in die proses gegenereer word moet verwyder word om die temperatuur in die brandstof te beperk.

The temperatuur van die brandstof moet beperk word om te verhoed dat klowingsprodukte in die omgewing vrygelaat word. Die temperatuur moet ook beperk word om te verhoed dat die grafiet nie spontaan oksideer in die teenwoordigheid van suurstof nie. Die brandstof word normaalweg in 'n helium omgewing geberg, maar daar moet aangetoon word dat die brandstof veilig is indien suurstof die ruimte sou binnedring.

Die doel van die studie is daarom om die temperatuur verdeling in die brandstof te bepaal vir verskillende toestande. Dit sluit geforseerde verkoeling in, en die moontlikheid van die passiewe verkoeling met behulp van natuurlike konveksie.

Berekeningsvloeimeganika (BVM) is gebruik om die verskillende hitte oordrag meganismes te simuleer. Dit sluit in warmte-oordrag tussen die vloeiers en die soliede oppervlakke, geleiding deur die soliedes en termiese straling tussen die oppervlaktes. Die effek van natuurlike konveksie is ook ingesluit omdat die pype deur die tenks die lugvloei verhoog as gevolg van die verhitting van die lug.

Die resultate toon dat die brandstof temperatuur nie die maksimum toelaatbare temperatuur oorskry tydens geforseerde verkoeling van 6 kg/s nie. Die moontlikheid om die tenk passief te verkoel lyk belowend, maar dit is baie afhanklik van die ontwerp van die skoorsteen. Die deurvloei area van die skoorsteen was die faktor wat die grootste effek op die massavloei deur die stelsel gehad het.

Die skoorsteen ontwerp en die ander dele van die stelsel wat nie in die studie ondersoek is nie, moet geanaliseer word alvorens die passiewe werking van die stelsel gewaarborg kan word.

# Table of Contents


Abstract ii

Uittreksel iv

Table of Contents vi

List of Figures viii

List of Tables x

Abbreviations xi

**CHAPTER ONE : INTRODUCTION ..... 1**

1.1 Background 1

1.2 Problem Statement: Analysis of Heat Removal 7

1.3 CFD as an Analysis Tool 8

1.4 Layout of Document 9

**CHAPTER TWO : GEOMETRY AND NUMERICAL MESH ..... 10**

2.1 Preamble 10

2.2 Geometry 11

2.3 Simplifications 11

2.4 Numerical Mesh 12

**CHAPTER THREE : MODEL IMPLEMENTATION ..... 14**

3.1 Assumptions 14

3.2 Different Cases Investigated 16

3.3 Materials Used and their Properties 17

3.4 Boundary Conditions 20

3.5 Energy Sources 25

3.6 Description of Chosen Numerical Models 25

**CHAPTER FOUR : MODEL INTERPRETATION AND DISCUSSION ..... 30**

4.1 Effect of Filling Level on Temperatures 30

4.2 Effect of Mass Flow Rate on Temperatures 31

4.3 Passive Flow without Chimney 32

4.4 Effect of Chimney on Passive Cooling Ability 33

**CHAPTER FIVE : VERIFICATION ..... 38**

5.1 Input Data Integrity 38

5.2 Simulation Integrity 38

5.3 Convergence 45

5.4 Summary 47

**CHAPTER SIX : CONCLUSION AND RECOMMENDATIONS ..... 48**

6.1 Conclusion 48

6.2 Recommendations 49

**REFERENCES ..... 50**

**APPENDIX A. : MATERIAL PROPERTIES ..... 53**

**APPENDIX B. : CALCULATIONS ..... 55**

**APPENDIX C. : EFFECT OF FILLING LEVEL ON RESULTS ..... 59**

**APPENDIX D. : EFFECT OF AIR MASS FLOW ON RESULTS ..... 69**

**APPENDIX E. : PASSIVE COOLING RESULTS ..... 74**

**APPENDIX F. : EFFECT OF CHIMNEY CROSS-SECTIONAL AREA ON RESULTS ..... 77**

**APPENDIX G. : EFFECT OF CHIMNEY LENGTH ON TEMPERATURE RESULTS ..... 79**

**APPENDIX H. : EFFECT OF CHIMNEY HEAT TRANSFER ON TEMPERATURE RESULTS ..... 80**

**APPENDIX I. : STAR-CD AND FLUENT COMPARISON ..... 82**

**APPENDIX J. : SIMULATION INTEGRITY CHECKS ..... 83**

# List of Figures


Figure 1: Layout of PBMR cycle [2]. 1
Figure 2: Relative size of fuel elements [2]. 3
Figure 3: Section of fuel element showing TRISO coated particle [2]. 4
Figure 4: Failure of containment vs. temperature [2]. 4
Figure 5: Decay heat of spent and used fuel [6]. 5
Figure 6: Used fuel tank geometry [13]. 10
Figure 7: Section of numerical mesh. 13
Figure 8: Air volume. 17
Figure 9: Helium volume. 18
Figure 10: Fuel volume. 19
Figure 11: Solid Volumes (not to scale). 20
Figure 12: Air inlet boundary. 23
Figure 13: Air outlet boundary – no chimney. 23
Figure 14: Air outlet boundary at chimney. 24
Figure 15: Effect of air mass flow on temperature results. 30
Figure 16: Effect of fill level on temperature results. 31
Figure 17: Effect of chimney cross-sectional area on temperature and mass flow results. 34
Figure 18: Piezometric pressure drop (relative) over chimney reduction. 35
Figure 19: Fuel temperature distribution comparison. 42
Figure 20: Typical heat flux convergence (Case A). 46
Figure 21: Calculation of effective conductivity. 57
Figure 22: Fuel temperature distribution. 60
Figure 23: Fuel temperature distribution – sections. 61
Figure 24: Tank temperature distribution. 62
Figure 25: Concrete temperature distribution. 63
Figure 26: Concrete temperature distribution – air outlet. 64
Figure 27: Concrete temperature distribution – support area. 64
Figure 28: Concrete temperature distribution – below support. 65
Figure 29: Concrete temperature distribution – defuel chute area. 66
Figure 30: Thermal shield temperature distribution. 67
Figure 31: Gamma radiation shield temperature distribution. 68
Figure 32: Fuel temperature distribution. 70
Figure 33: Fuel temperature distribution – sections. 71
Figure 34: Tank temperature distribution. 72
Figure 35: Concrete temperature distribution. 73
Figure 36: Fuel temperature distribution. 74
Figure 37: Tank temperature distribution. 75

Figure 38: Concrete temperature distribution. 76
Figure 39: Piezometric pressure contour plot showing pressure drop over chimney reduction. 78
Figure 40: Effect of chimney length on temperature results for 100% filled tank. 79
Figure 41: Effect of chimney length on temperature results for 20% filled tank. 79
Figure 42: Effect of chimney heat transfer on temperature results for 100% filled tank. 80
Figure 43: Effect of chimney heat transfer on temperature results for 20% filled tank. 80
Figure 44: Tank temperature distribution comparison. 82
Figure 45: Concrete temperature distribution. 82

# List of Tables


Table 1: Summary of numerical cells used. 12

Table 2: Cases investigated. 16

Table 3: Fuel volumes. 19

Table 4: Common inlet conditions 21

Table 5: Inlet and outlet conditions for different models. 21

Table 6: Wall boundary conditions. 24

Table 7: Applied heat sources. 25

Table 8: Porous media characteristics 28

Table 9: Results for passive operation without chimney. 32

Table 10: Effect of chimney length on mass flow and maximum temperatures. 36

Table 11: Effect of chimney heat transfer on mass flow and maximum temperatures. 37

Table 12: Comparative temperature results. 43

Table 13: Surface heat transfer comparison. 44

Table 14: Y-plus value summary. 45

Table 15: Material properties of air. 53

Table 16: Material properties of helium. 53

Table 17: Material properties of fuel. 54

Table 18: Material properties of tank. 54

Table 19: Material properties of concrete. 54

Table 20: Material properties of shield. 54

Table 21: Material properties of gamma shield. 54

Table 22: Calculation of effective conductivity of thermal shield. 58

Table 23: Effect of filling level on maximum temperatures. 59

Table 24: Effect of air mass flow on maximum temperatures. 69

Table 25: Effect of chimney area reduction on maximum temperatures. 77

Table 26: Chimney wall heat transfer. 81

Table 27: Y-plus values on important surfaces. 83

Table 28: Energy balance of different cases. 84

# Abbreviations

| | |
|---|---|
| BNFL | British Nuclear Fuel |
| CFD | Computational Fluid Dynamics |
| FEM | Finite Element Method |
| FHSS | Fuel Handling and Storage System |
| FV | Finite Volume |
| HTR | High-temperature Reactor |
| HVAC | Heating, Ventilation and Air-conditioning |
| IDC | Inustrial Development Corporation |
| LEU | Low Enriched Uranium |
| LWR | Light Water Reactor |
| n/a | Not Applicable |
| PCU | Power Conversion Unit |
| PBMR | Pebble Bed Modular Reactor |
| QA | Quality Assurance |
| QAP | Quality Assurance Procedure |
| SIMPLE | Semi Implicit Method for Pressure Linked Equations |
| THTR | Thorium High-temperature Reactor |
| TRISO | Triple Coated Particle |
| UFT | Used Fuel Tank |

different temperatures. For temperatures below 1 600 °C, the failure rate is so low that no significant radiological release of fission products occurs [5]. The geometry of the reactor is chosen specifically to limit the maximum fuel temperature to below 1 600 °C for loss of coolant events.

The fuel kernels in the graphite matrix are shown on the left-hand side of Figure 3. The distribution of the kernels in the graphite lowers the power density of the fuel element and increases the heat capacitance of the element. The high heat capacitance and low power density reduce the thermal response of the fuel element. The thermal response of the system is therefore slow enough to allow human interference.

### 1.1.3 Storage of fuel

Once the fuel has made one cycle through the reactor, it generates decay heat due to the decay of the fission products. If the fuel is not returned to the reactor where it is at its safest, it should be stored in a storage vessel capable of removing the decay heat to limit the fuel temperature during storage.

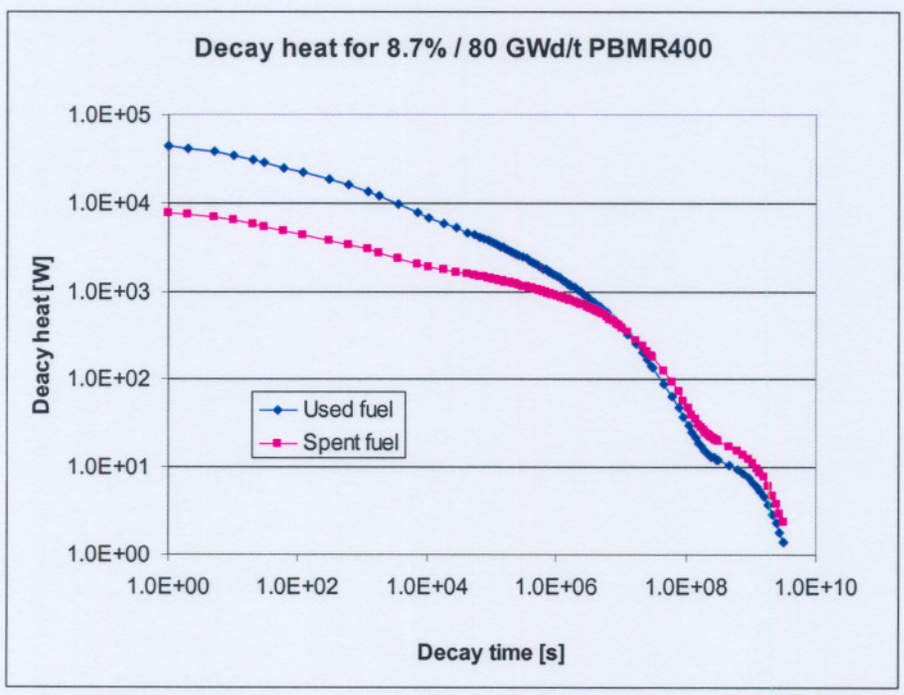


**Figure 5: Decay heat of spent and used fuel [6].**

There are currently two different scenarios of fuel storage:

- Storage of spent fuel.
- Storage of used fuel.

The heat generated per fuel element for the spent and used fuel is shown in Figure 5.

As mentioned previously, spent fuel is fuel that has reached the burn-up limit of 80 000 MW.d/$t_{uranium}$. This type of fuel will be loaded continuously into the storage tank during normal operation. The number of fuel elements used each day is 484, and it would therefore take approximately 3.4 years to fill one tank capable of storing 600 000 fuel elements. The fuel is stored in these tanks for a further 40 years after the plant has been shut down before it is removed for final storage and the decommissioning of the building.

Used fuel, on the other hand, is a mixture of fresh and used fuel. This type of fuel should be stored when all the fuel is removed from the reactor for repairs to be done inside the reactor. The used fuel produces more decay heat per fuel element than the spent fuel [6], and the tank is filled in a shorter period of time. The filling of the tank should typically start about four days after shutdown, and it typically takes 20 days to fill the tank.

The net effect is that the total heat load on the tank is much higher because the fuel in the tank is fresher, with more decay heat being generated per fuel element. The time the fuel is stored in the used fuel tank is much shorter than in the case of the spent fuel. As mentioned earlier, the spent fuel is stored for a further 40 years after plant operation is stopped, while the fuel in the used fuel tank is returned to the reactor after the maintenance has been completed. Although the heat load on the used fuel tank is higher, the requirement regarding the operational life of the tanks is shorter.

As mentioned previously, the fuel should be kept below 1 650 °C to limit the release of fission products. A further constraint on the safe storage of the fuel is the temperature where graphite may start to oxidize in the presence of oxygen. This limit is currently specified as 400 °C [7]. The fuel must be stored

at a temperature below this value at all times to ensure the safety of the fuel and its fission products, should large amounts of oxygen come into contact with them.

The thermo-hydraulic analysis of the tank is therefore very important to determine the temperature distribution in the fuel and the tank components. The remainder of this document will therefore focus on the thermal analysis of the used fuel storage tank.

## 1.2 Problem Statement: Analysis of Heat Removal

The accurate prediction of the peak or maximum fuel temperature is extremely important when different storage concepts are evaluated. This is required to prove that the fuel will be maintained at conditions that would not result in the breaking of the primary containment, in this case the coatings around the fuel, and increased fission product release. There are a number of ways in which this and other important thermo-hydraulic design parameters can be determined, including the following:

- Building of experimental test rigs.
- Use of actual plant data.
- Development of analytical models based on empirical data.
- Integrated solution of all important mechanisms.

Being in the concept phase, the building of experimental test rigs can be very expensive and time-consuming. It is therefore believed that this approach will not form part of the concept or basic design phase.

The layouts proposed for the German reactors are very expensive because the amount of fuel stored in each canister is very small, making the entire storage approach very uneconomical [8]. This led to the design of a different layout, and as a result, no plant data is available for use in the design process. Once the current layout is constructed, the data obtained from it can be used to verify the calculations done in the design before the storage tanks are filled to the limit.

Analytical models based on empirical data definitely have merit. The benefits include the simplification of the actual geometry to cases where analytical data is available. The problem with this approach is that it can be used to do initial scoping calculations, but the moment more detail is required, the assumptions that must be made may invalidate the results. The amount of bookkeeping required to ensure that the vast numbers of equations involved are set up and solved correctly, can be immense.

The last option is to make use of an integrated solution methodology that is able to address most of the detail involved without bombarding the analyst with the finer detail of the solution methodology. The Finite Element Method (FEM) and Finite Volume method (FV) are but two methods currently used to facilitate the integrated solution of various physical phenomena.

The purpose of this study is therefore to determine the temperature distribution in the fuel and the components of the used fuel tank for different scenarios with an appropriate analysis tool.

## 1.3 CFD as an Analysis Tool

The analysis tool used should be able to model the following major heat transfer characteristics:

- Conduction.
- Convection.
- Thermal radiation.

Although most FEM codes do have the capability to model fluid flow [9], FV has historically been used for the PBMR. Most of the commercial FEM codes also have only limited capabilities when it comes to the solution and set-up of thermal radiation.

The FV code STAR-CD currently being used for the PBMR, has the capability to model all three of the major heat transfer mechanisms mentioned in detail [10]. This, and the fact that the geometry under consideration can be modelled in detail, makes it a very attractive solution methodology.

CFD was used in the past to model storage tanks, but the geometry investigated was very different compared to the current proposed layout, and the extent of the boundaries was much more limited [11]. The boundaries were typically fixed on the outer surface of the canister to determine the effects within the tank, while it was assumed that the environment surrounding the tank was kept constant.

It was therefore decided to make use of the CFD code STAR-CD to build a detail model of the current used fuel tank geometry, and to use the code's capabilities to model the three heat transfer mechanisms mentioned.

## 1.4 Layout of Document

The layout of the document is arranged around the methodology of setting up a CFD model. The geometry and the numerical mesh that are created are therefore dealt with in Chapter Two. In Chapter Three, the implementation of the model, including aspects such as the material properties and the different solution settings, are discussed. In Chapter Four, the results obtained are presented and analysed, and the validity of the results is addressed in Chapter Five by comparing it to results of another code. The conclusions drawn from the results and recommendations made are presented in Chapter Six.

# CHAPTER TWO: GEOMETRY AND NUMERICAL MESH

In this chapter, the geometry under investigation is shown and the simplifications made to ease the modelling thereof are highlighted. The numerical mesh is also shown and discussed briefly.

## 2.1 Preamble

The used fuel tank is basically a tank with pipes running from the top to the bottom through the tank. The purpose of the pipes is to allow the air passing through them to cool the contents of the tank. The pipes act as chimneys, as they are heated by the fuel surrounding them. The pipes are spaced in such a way to ensure that the fuel inside the core stays subcritical [12].

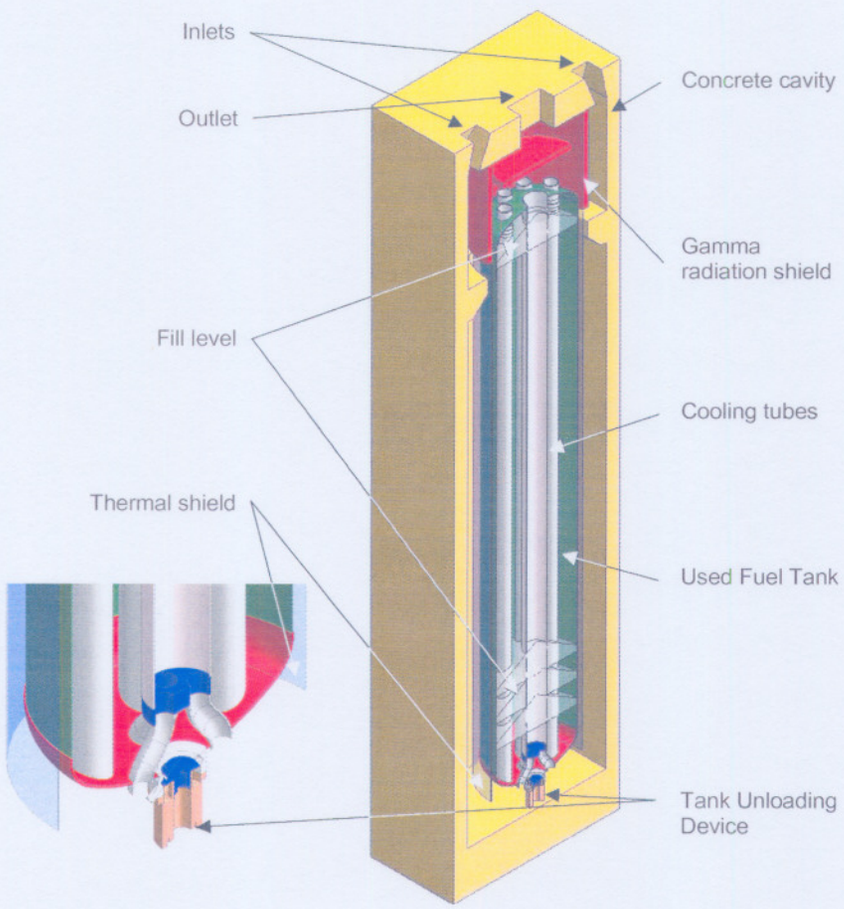


**Figure 6: Used fuel tank geometry [13].**

## 2.2 Geometry

A 180° section of the geometry under investigation is shown in Figure 6. The figure shows the tank as it is situated in the concrete cavity. The tank with the centre pipe and the eight pipes around it can be seen. The different filling levels investigated in this study are also indicated as cones. The area around the tank will be cooled by air entering and leaving the cavity at the inlets and outlet shown. The volume in the cavity will be filled with helium, because the Fuel Handling and Storage System (FHSS) is operated using helium.

## 2.3 Simplifications

The following simplifications were made to the geometry to ease the modelling of the geometry:

a. 90° section with symmetry planes

   The symmetry that exists around the centreline of the model is such that it was possible to use only a 90° section of the geometry for the model. Figure 6 shows a 180° section of the geometry.

b. Tank unloading device

   Some detail of the tank unloading device can be seen in Figure 6. This level of detail is not required for the thermo-hydraulic analysis of the tank, and it was therefore decided to simplify it by using the outlines of the component, and to assume that it is a solid piece of material.

c. Compensators not included

   The compensators present on the pipes to relieve the stresses in the pipes due to thermal expansion were ignored.

d. Thermal radiation shield

   The thermal radiation shield consists of three layers. The inner layer is steel and the outer layer is aluminium foil. Between the two layers is a layer of glass wool that acts as thermal insulation. This composite shield is represented with a single material with the effective conductivity of the three layers.

e. No protection on concrete at HVAC outlet

The high outlet temperature of the air necessitates the use of some kind of protection for the concrete at the HVAC outlet. This protection was not included in the model.

f. Inlets and outlets

The chimney at the outlet of the model and the header at the inlet are ignored in this model, because the flow at the inlet was fixed to a specific mass flow rate. The effect of the chimney on the passive flow models forms part of this investigation.

g. Chimney modelled without bends

The bends and other components will add additional pressure losses to the system. The models will, however, give an initial indication of the viability of operating the system with buoyancy driven flow.

## 2.4 Numerical Mesh

The numerical mesh was constructed in GAMBIT 2.0. This software forms part of the FLUENT family of codes. It is basically a meshing tool with advanced auto meshing capabilities. The software is capable of creating 3D meshes of complex geometries, but the user should still subdivide the geometry into smaller sections to ease the meshing process and to ensure a good quality mesh. The user is allowed to make use of a number of cell types, including hexahedral, tetrahedral and prism cells [14].

Table 1 summarizes the number of cells used for the solids and the fluids.

**Table 1: Summary of numerical cells used.**

| Solid | Fluid | Total |
|---|---|---|
| 138 636 | 497 982 | 636 618 |

Figure 7 shows the mixed use of hexahedral and tetrahedral cells in parts of the numerical mesh. The outlines of the tank can be clearly seen in the figure.

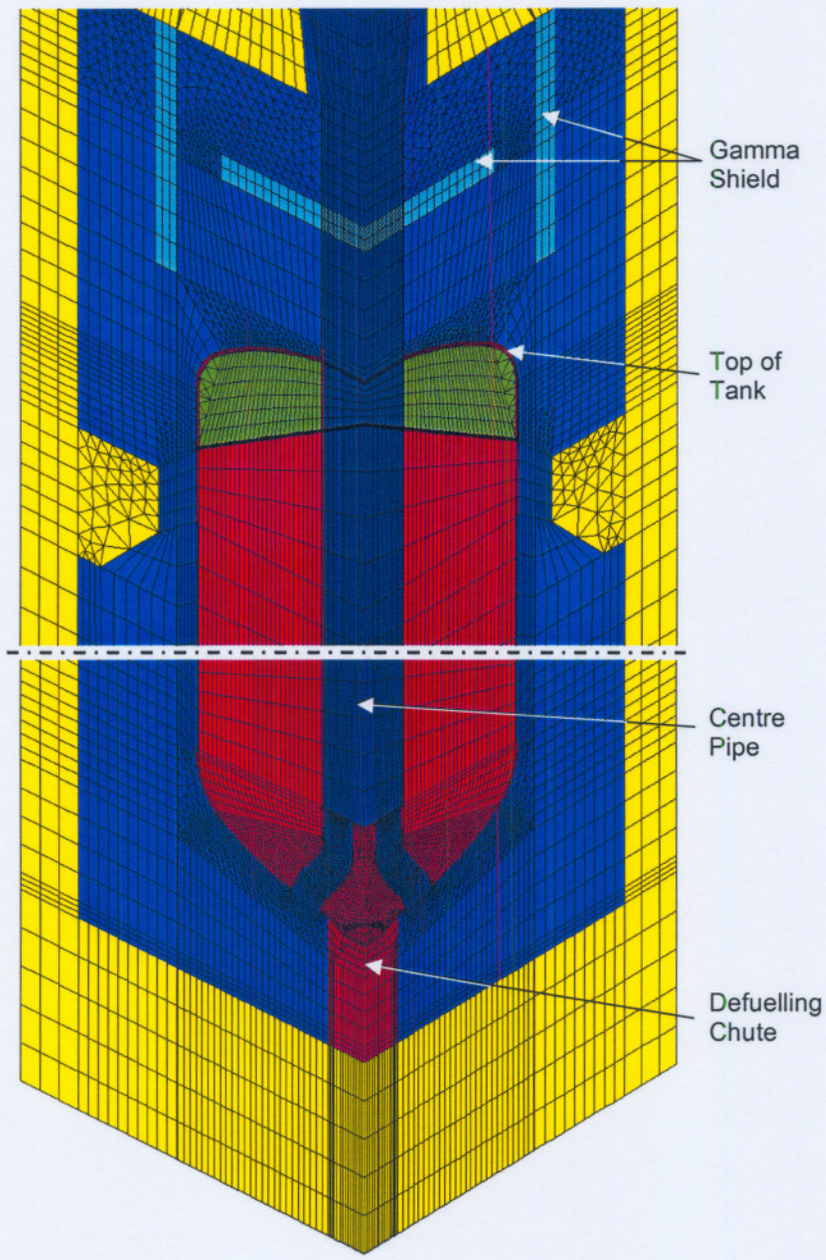


**Figure 7: Section of numerical mesh.**

# CHAPTER THREE: MODEL IMPLEMENTATION

This chapter highlights the implementation of the model in the CFD code STAR-CD, including the major assumptions made. The relevant boundary conditions and settings required by the code are also discussed.

## 3.1 Assumptions

Due to the complexity of the model, assumptions had to be made in the modelling of the tank and its components. These assumptions include the following:

a. Contact resistance between solids

The contact resistance between the different solids in contact with each other is ignored. It is assumed that the solids make 100% contact on the surfaces exposed to each other. The influence of this assumption should be minimal because the areas where solids are in contact with each other are very small, and do not form an integral part of the main heat removal path.

b. Effective conductivity of fuel pebbles

The fuel is made up of spheres, and it is therefore incorrect to use the material properties of the fuel only to model the heat transfer. The difficulty lies in the fact that the conductivity of the fuel is made up of three different heat transfer mechanisms, namely the conduction through the bed, the radiation between pebbles, and the convection of the gas filling the cavities between the pebbles. An effective conductivity is therefore used to model the combined effect of all the heat transfer mechanisms [15].

c. Porosity of fuel pebbles

The porosity of the fuel is assumed to be 0.39, the same porosity value that is used for the reactor models. The porosity may, however, be larger due to the fact that the bed is penetrated by the cooling tubes, increasing

the number of pebbles in contact with a flat surface. This effect should be investigated in further studies.

d. Conduction of pebble not taken into consideration

The conduction of heat from the centre of the pebble to the surface of the pebble is not taken into consideration because of the small temperature gradient if the heat generation in the pebble is due to decay heat only. A first order calculation is shown in Appendix B.1.

e. Solid layer on fuel for radiation purposes

A thin graphite layer represents the top surface of the fuel. The reason for this layer is to include the effect of radiation from this surface to the inside of the tank [16].

f. Outer concrete surface temperature

The effect of the other cavities on this cavity is ignored. The outer surface of the concrete is therefore fixed at 35 °C. The effect of this assumption should be verified with an integrated simulation of the entire storage area.

## 3.2 Different Cases Investigated

Table 2 gives a summary of the different cases investigated in this study. It shows the major differences between the models. A more detailed description of the relevant boundary conditions is given in section 3.4.

**Table 2: Cases investigated.**

| Case | Name | Description | | Chimney | | |
|---|---|---|---|---|---|---|
| | | Fill level (%) | HVAC (kg/s) | Area (m*m) | Length (m) | Heat Transfer ($W/m^2.K$) |
| A | uft-r2-10% | 10 | 6 | None | - | - |
| B | uft-r2-15% | 15 | 6 | | - | - |
| C | uft-r2-20% | 20 | 6 | None | - | - |
| D | uft-r2-100% | 100 | 6 | None | - | - |
| E | uft-r2-20%-3kgs | 20 | 3 | None | - | - |
| F | uft-r2-20%-8kgs | 20 | 8 | None | - | - |
| G | uft-r2-20%-passive | 20 | Passive | None | - | - |
| H | uft-r2-100%-passive | 100 | Passive | None | - | - |
| I | uft-r2-100%-chimney-passive | 100 | Passive | 0.5*0.4 | 27 | 0 |
| J | uft-r2-100%-chimney-2-passive | 100 | Passive | 1.2*1.2 | 27 | 0 |
| K | uft-r2-20%-chimney-3-passive | 20 | Passive | 0.8*0.6 | 27 | 0 |
| L | uft-r2-100%-chimney-3-passive | 100 | Passive | 0.8*0.6 | 27 | 0 |
| M | uft-r2-20%-chimney-4-passive | 20 | Passive | 0.8*0.6 | 15 | 0 |
| N | uft-r2-100%-chimney-4-passive | 100 | Passive | 0.8*0.6 | 15 | 0 |
| O | uft-r2-20%-chimney-5-passive | 20 | Passive | 0.8*0.6 | 27 | 5 |
| P | uft-r2-100%-chimney-5-passive | 100 | Passive | 0.8*0.6 | 27 | 5 |
| Q | uft-r2-15%-solid | 15 | 6 | None | - | - |

## 3.3 Materials Used and their Properties

The following paragraphs show the different volumes found in the model, the material assigned to the volumes, and their properties. The materials given in [13] were used as far as possible, but where they differ from the PBMR materials database [17], the latter was used.

### 3.3.1 Air

Figure 8 shows the geometry of the air as it is modelled. The details of the material properties used for the air are shown in Table 1 in Appendix A.

**Figure 8: Air volume.**

### 3.3.2 Helium

The different filling levels of the tank result in different helium volumes above the fuel. The flow in the helium is driven only by natural convection, and it therefore acts as a cooling medium for the top surface of the fuel. The different helium volumes for the different filling levels can be seen in Figure 9. The material properties used for the helium are shown in Table 16 in Appendix A.

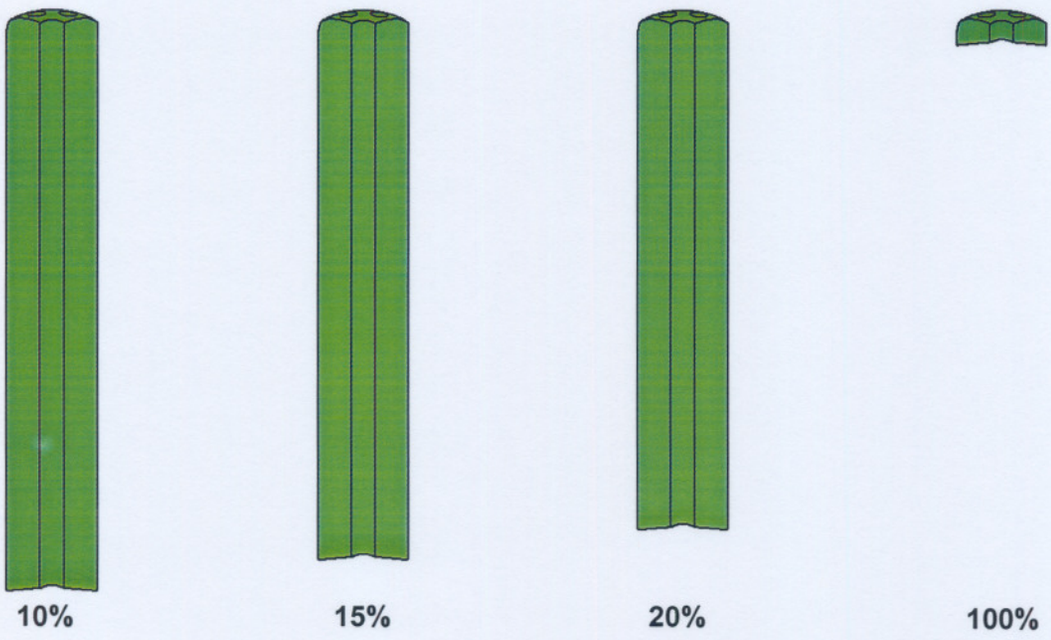


**Figure 9: Helium volume.**

### 3.3.3 Fuel

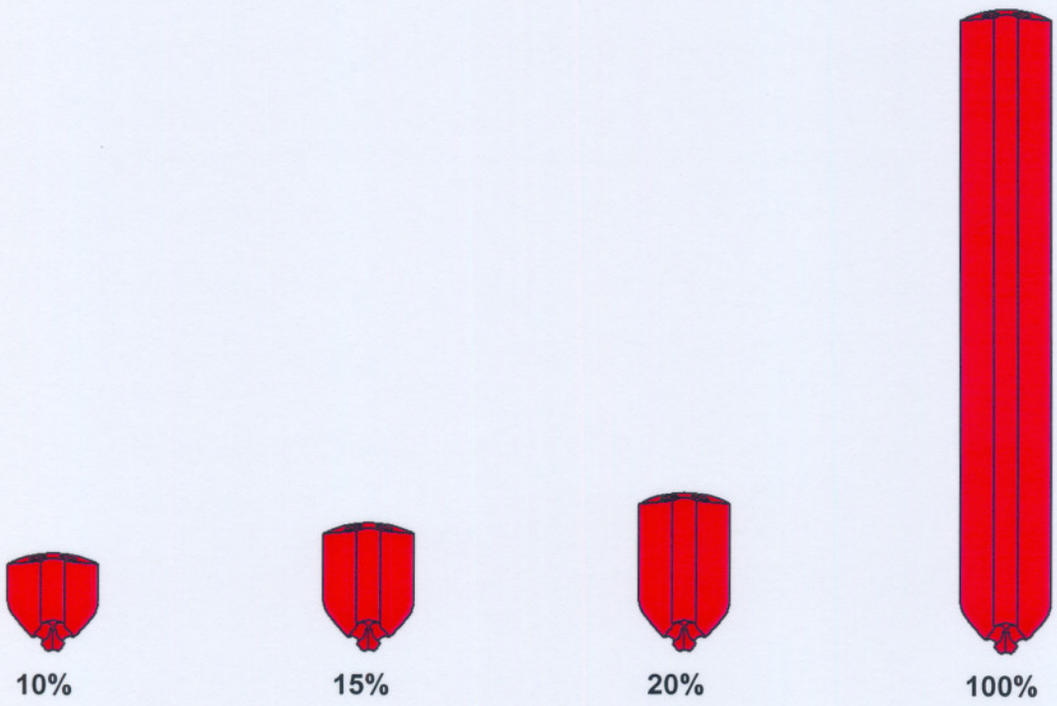


**Figure 10: Fuel volume.**

The fuel volumes for the different filling levels are shown in Figure 10 and Table 3. The fuel is modelled as a porous region with an effective conductivity that includes the heat transfer mechanisms such as point conduction and radiation between the pebbles. The effective conductivity is based on the method of Zehner and Schlünder [15].

**Table 3: Fuel volumes.**

| Case | Fill Height | Calculated Volume1 |
|---|---|---|
| uft-r2-10% | 10% | 8.6 |
| uft-r2-15% | 15% | 12.9 |
| uft-r2-20% | 20% | 17.2 |
| uft-r2-100% | 100% | 85.8 |

[1] Volume calculation based on volumes of numerical mesh.

### 3.3.4 Solids

The solids included in the CFD model are shown in Figure 11. Conduction through the solids and radiation from most of the solid surfaces are solved.

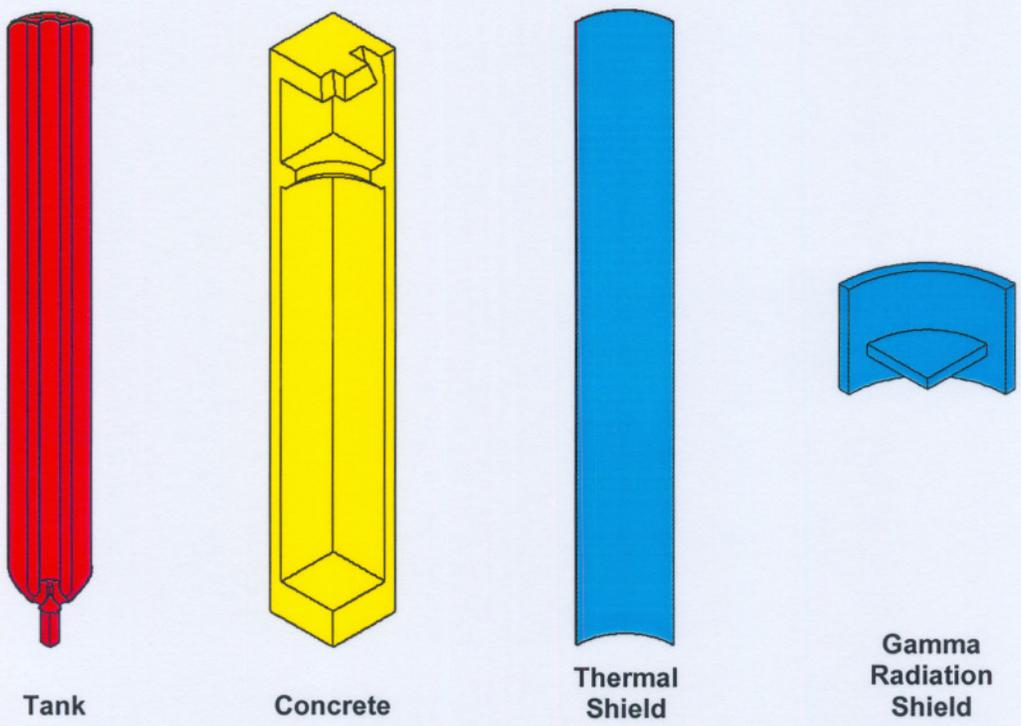


**Figure 11: Solid Volumes (not to scale).**

The calculation of the properties of the thermal shield is presented in Appendix B.2. This represents an effective conductivity to use instead of specifying the different layers in the CFD model. By following this approach, the number of computational cells required is reduced.

The material properties used for the rest of the solids are given in Appendix A.

## 3.4 Boundary Conditions

The boundary conditions of the models are required to differentiate between the operating conditions investigated.

The location of the air inlet and outlet boundaries is shown in Figure 12 to Figure 14. The mass flow of the inlet boundary is either varied according to the operating condition investigated, or set as pressure boundaries to simulate

passive operation. In Figure 12, the boundary is indicated as a fixed mass flow boundary representing forced flow.

The HVAC inlet conditions, which were kept constant for all of the analyses, are shown in Table 4. The conditions that were changed for the different models are shown in Table 5.

**Table 4: Common inlet conditions**

| Parameter | Value | Unit |
|---|---|---|
| Temperature | 35 | °C |
| Turbulence intensity | 10 | % |
| Mixing length | 0.06 | m |

The specifications of the inlet and outlet boundary conditions fit into two categories according to Table 5. They are:

- Fixed mass flow conditions.
- Passive flow with pressure specified at boundaries.

**Table 5: Inlet and outlet conditions for different models.**

| Case | Description | Inlet | | Outlet | |
|---|---|---|---|---|---|
| | | Type | Value | Type | Value |
| A - D | Fixed mass flow, 6 kg/s | Inlet | 6 kg/s | Outlet | n/a |
| E | Fixed mass flow, 3 kg/s | Inlet | 3 kg/s | Outlet | n/a |
| F | Fixed mass flow, 8 kg/s | Inlet | 8 kg/s | Outlet | n/a |
| G - H | Passive flow | Pressure (piezometric) | 101.3 kPa | Pressure (piezometric) | 101.3 kPa |
| I - P | Passive flow with chimney | Pressure (piezometric) | 101.3 kPa | Pressure (piezometric) | 101.3 kPa |
| Q | Fixed mass flow, 6 kg/s | Inlet | 6 kg/s | Outlet | n/a |

The pressure specified for the passive flow cases is the piezometric pressure. The relation between piezometric and total pressure is [18]:

$$P = P_T - \rho \cdot g \cdot h - \frac{1}{2}\rho V^2 \qquad [1]$$

with:

| | | |
|---|---|---|
| P | : | Piezometric pressure |
| $P_T$ | : | Total pressure |
| $\rho$ | : | Density of fluid |
| g | : | Gravitational acceleration |
| h | : | Height from a reference point |
| V | : | Velocity of fluid |

By specifying the piezometric pressure at the inlet and outlet for the passive operation cases, the code is allowed to calculate the true static pressure at the corresponding reference height of the boundary. The reason the piezometric pressures at the inlet and outlet are set equal is because no external source is applied to force the fluid through the domain.

The reference height for the buoyancy calculation was specified at the inlet for all of the models. The reference density at this height was calculated at the inlet conditions of 101.3 kPa and 35 °C to be 1.1454 kg/m$^3$.

### 3.4.1 Inlet boundary position

The position of the air inlet is shown in Figure 12. The location of this boundary was kept constant for all the calculations, although the type of boundary was varied to suit the specific flow condition.

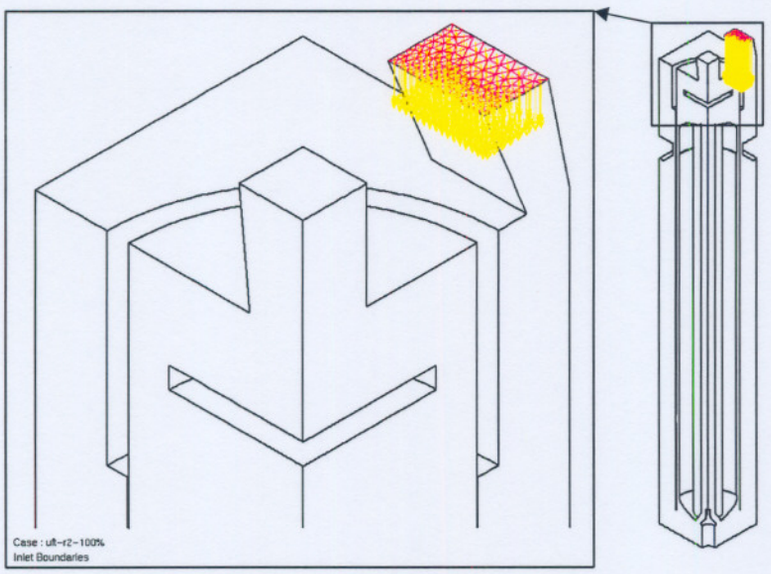


**Figure 12: Air inlet boundary.**

### 3.4.2 Outlet boundary position

The location of the outlet boundary for the cases without and with a chimney is shown in Figure 13 and Figure 14 respectively.

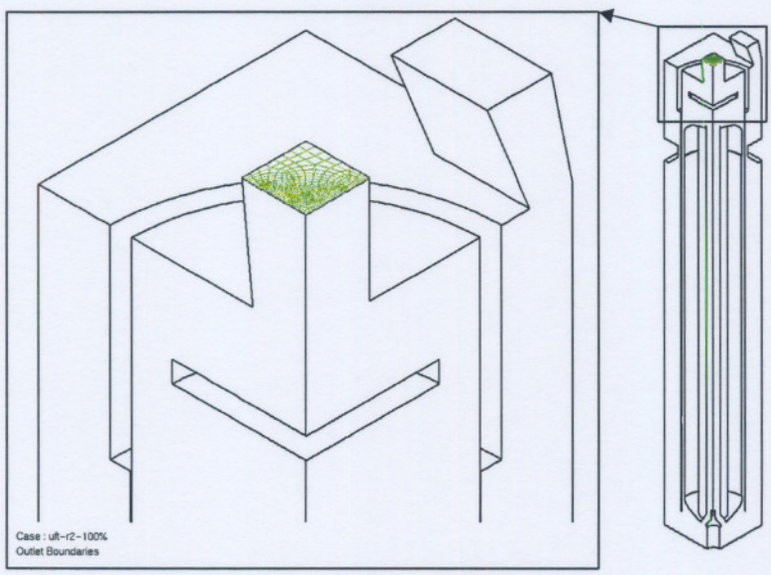


**Figure 13: Air outlet boundary – no chimney.**

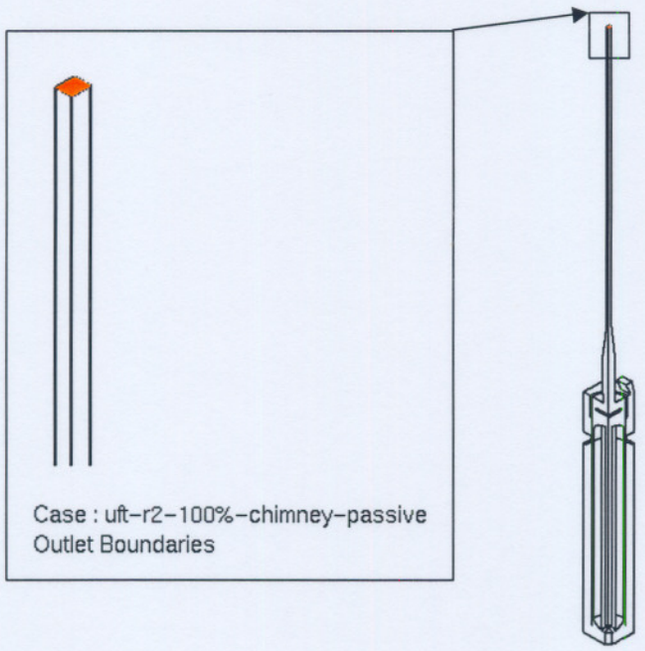


**Figure 14: Air outlet boundary at chimney.**

### 3.4.3 Wall boundary conditions

The boundary conditions on the walls were treated as conducting boundaries. This means that heat transfer between the solids and the fluids is taken into consideration.

**Table 6: Wall boundary conditions.**

| Surface | Temperature (°C) | Heat Transfer Coefficient ($W/m^2.K$) | Emissivity |
|---|---|---|---|
| Tank Inner Surface | - | - | 0.29 |
| Tank Outer Surface | - | - | 0.29 |
| Fuel Surface | - | - | 0.88 |
| Thermal Shield Inner Surface | - | - | 0.88 |
| Thermal Shield Outer Surface | - | - | 0.05 |
| Gamma Radiation Inner Surface | - | - | 0.1 |
| Gamma Radiation Outer Surface | - | - | 0.1 |
| Inner Concrete Surface | - | - | 0.91 |
| Outer Concrete Surface | 35 | - | - |
| Chimney Surface[2] | 20 | 5 | - |

[2] Only applied in the case where chimney heat transfer is investigated.

The boundary is also used to fix the temperature on a surface, if required, and to specify the thermal radiation properties of the surface. The wall boundaries specified are shown in Table 6.

## 3.5 Energy Sources

The decay heat generated within the fuel is specified as an enthalpy source through user coding. It is assumed that the decay heat starts once the nuclear reaction stops, and that all the fuel elements will therefore generate the same amount of decay heat. The decay heat is therefore only a function of the time since shutdown. The heat source specified in the model is therefore dependent on the filling height only, and is assumed to be constant through the entire fuel volume.

The applied heat sources are shown in Table 7 [13].

**Table 7: Applied heat sources.**

| Filling Height (%) | Heat Input ($W/m^3$) |
|---|---|
| 10 | 10 240 |
| 15 | 9 921 |
| 20 | 9 602 |
| 100 | 6 791 |

The source is specified as $W/m^3$. The code applies this source explicitly in each of the computational cells, and calculates the energy as function of the cell volume.

## 3.6 Description of Chosen Numerical Models

### 3.6.1 Conservation equations

The following equations were solved in all of the cases investigated:

- Continuity conservation.
- Momentum conservation.
- Energy conservation.

These are the standard conservation equations solved for in a CFD analysis involving heat transfer [10].

### 3.6.2 Turbulence

The standard k-ε-turbulence model was used in all of the simulations because the flow is fully turbulent for most of the domain. The flow through the pipes is of utmost importance, and in these areas the flow is fully turbulent.

Wall functions were used to represent the boundary layer on the solid surfaces. The accuracy of the result is very much dependent on the y-plus value when wall functions are used. This places an additional restriction on the size of the cells in the boundary layer. The y-plus value calculated should be in the range 30 to 100 for accurate results [10], while values up to 500 may still give acceptable results for in-pipe flows [19].

### 3.6.3 Thermal radiation

Thermal radiation is energy emitted by materials that are at a finite temperature. This is an important heat transfer mechanism in most heat transfer problems where surfaces are at different temperatures and convection are involved [20]. The expected temperature of the fuel is in the region of 250 °C to 350 °C based on previous concepts analysed [21], and it was therefore decided to include the effect of radiation.

In STAR-CD, the option exists to calculate the following thermal radiation phenomena:

- Radiation between surfaces only.
- Radiation between surfaces and the fluids/gases between them (participating media).

Gaseous radiation is very limited in the case of air. The reason for this is that air consists mainly of nitrogen ($N_2$) and oxygen ($O_2$), which are nonpolar and therefore do not emit any radiation, and are essentially transparent to incident radiation [22]. The effect of radiation on the air is therefore ignored in this analysis.

Radiation between surfaces is calculated in STAR-CD by subdividing all the surfaces involved in thermal radiation into smaller regions or patches. The view factor required to calculate the incident and emitted radiation from each of these patches is obtained during a view factor calculation, before the actual solution. The view factor is calculated by emitting a number of beams from each patch, and monitoring which patches it intercepts. In this way all patches taking part in the radiation exchange from the patch emitting the beam are identified before the actual view factor calculation for each patch starts.

The actual properties of the surface are set by specifying the emissivity and absorbtivity of the patches. This is done per boundary region, and it is therefore important to specify different boundary regions for surfaces with different radiation properties.

### 3.6.4 Porous medium

The use of porous media in the analysis of packed beds with internal heat generation is a methodology that has received much attention [23]. The modelling of the pebble bed using CFD is also based on the use of porous media to model the effect of the distributed resistance of the pebbles [24]. The reason a porous medium is used to model the pebble bed is to reduce the number of numerical cells required. This is necessary because the number of pebbles in the reactor is in the order of 400 000, and a vast number of cells will be required if the detail of the pebbles is included.

The modelling of porous media is a standard capability of STAR-CD. The distributed resistance can be variable in the three axis directions of any one of the local coordinate systems specified in the pre-processor. The equation for the distributed resistance is shown in equation [2] (from reference [10]):

$$-K_i u_i = \frac{\partial p}{\partial \xi_i} \qquad [2]$$

where

- $\xi i$ (i=1,2,3) represents the (mutually orthogonal) orthotropic directions
- $K_i$ is the permeability
- $u_i$ is the superficial velocity in direction $\xi i$

The permeability $K_i$ is assumed to be a function of the superficial velocity magnitude $\bar{v}$ as shown in equation [3] (from reference [10]):

$$K_i = \alpha_i \left|\bar{v}\right| + \beta_i \qquad [3]$$

with $\alpha_i$ and $\beta_i$ user-supplied coefficients. The superficial velocity is defined as the total volume flow rate divided by the total cross-sectional area of the fluid and the solid.

The values used in the model are based on the values used in the CFD models of the reactor, and are presented in Table 8 [24]. The values are assumed to be isotropic.

**Table 8: Porous media characteristics**

| Variable | Value |
|---|---|
| Alpha | 650 |
| Beta | 110 |

### 3.6.5 Discretisation scheme

The discretisation schemes chosen are as follow:

- Momentum : MARS
- Turbulence : Upwind Differencing
- Temperature : Upwind Differencing
- Density : MARS

Due to the complexity of solving buoyancy driven flow, it was decided to make use of a higher order discretisation to solve the momentum and density equations.

### 3.6.6 Solver

The SIMPLE (Semi Implicit Method for Pressure Linked Equations) algorithm was used as the default solution method in all instances. The effect of using different solver algorithms was not studied.

# CHAPTER FOUR: MODEL INTERPRETATION AND DISCUSSION

This chapter gives a summary of the results obtained. Due to the volume of the results presented, only the most important results are shown and discussed, with the rest being presented in the appendices.

## 4.1 Effect of Filling Level on Temperatures

The effect of the level to which the tank is filled on the maximum temperatures of selected components is shown in Figure 15. Two things occur as the tank is being filled:

- The total heat load on the system increases as the number of pebbles increase.
- The heat density reduces due to the decrease of the decay heat with time.

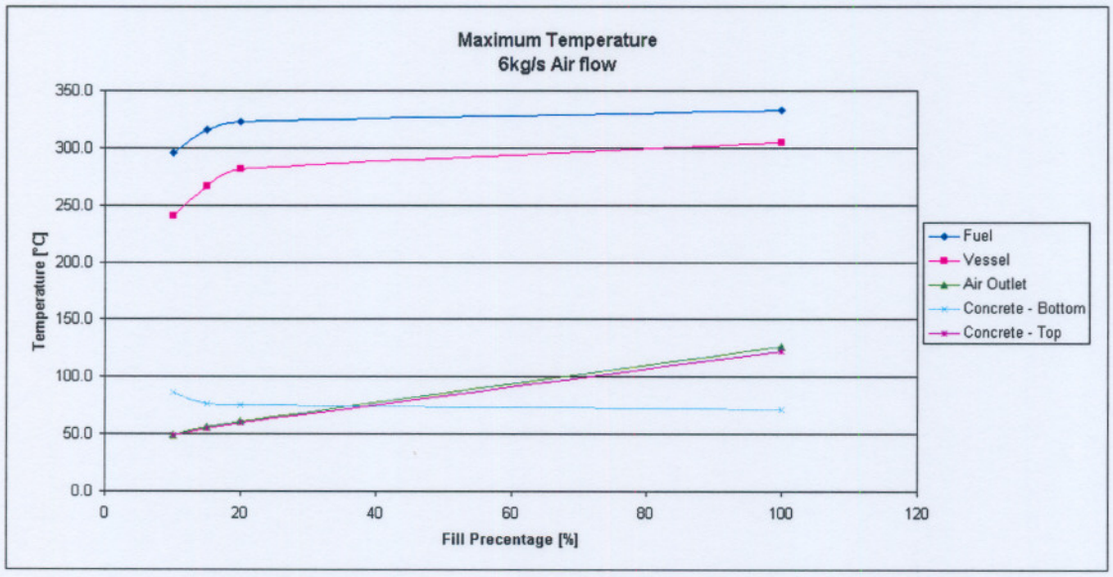


**Figure 15: Effect of air mass flow on temperature results.**

The fuel volume increases linearly because the filling rate is constant, while the decay heat reduces exponentially. From the above it is evident that the heat load on the system does not increase linearly with time.

Figure 15 shows that based on the cases investigated, the temperatures of the fuel and vessel increase quickly to the 20% filling level, from where they only increase slightly to the 100% filling level.

The concrete follows a different trend. The temperature of the concrete at the bottom decreases as the tank is filled, because the decay heat reduces at the same time. The temperature of the concrete at the top increases as the tank is filled, because the total heat load on the system increases while the mass flow of the air stays constant. As can be seen from the figure, this leads to an increase in the outlet temperature of the air.

In Appendix C, the results are listed in tabular form in Table 23, and the temperature contour plots of the components are shown in Figure 22 to Figure 31.

## 4.2 Effect of Mass Flow Rate on Temperatures

The effect of varying the air mass flow can be seen in Figure 16. From this figure it is clear that the overall effect is that the maximum temperatures of the components reduce when the air mass flow is increased. It can also be seen that the maximum fuel temperature approaches the safety limit of 400 °C [6] when the specified air mass flow is 3 kg/s.

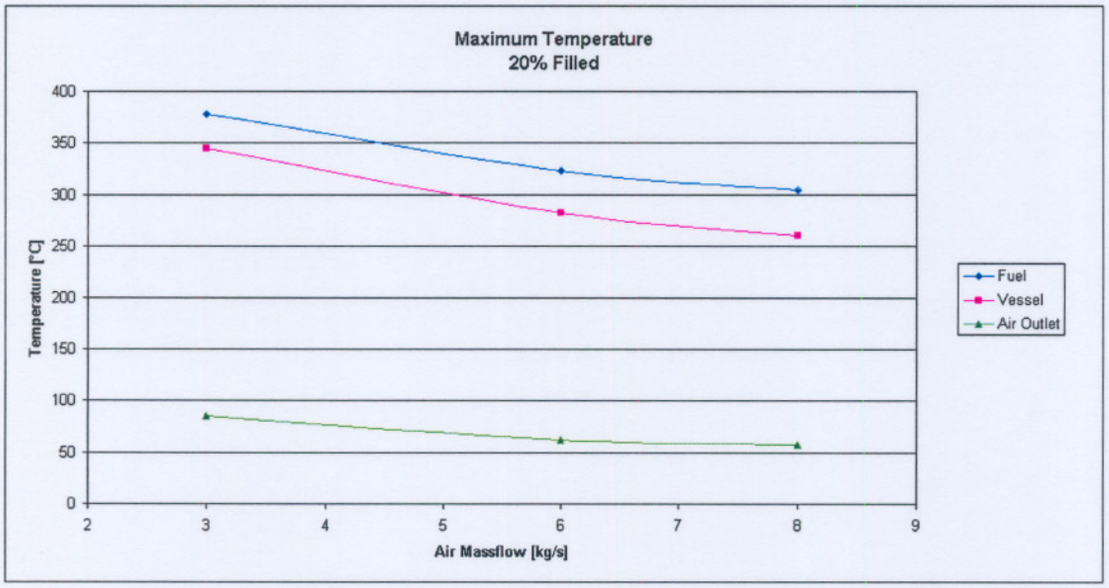


**Figure 16: Effect of fill level on temperature results.**

This indicates that the lower limit on the air mass flow is in the order of 3 kg/s. This result should be kept in mind when the passive operation of the tanks is investigated.

It can be seen from Figure 16 that there is a significant decrease in the temperatures from 3 kg/s to 6 kg/s air mass flow, but that the decrease is not that significant from 6 kg/s to 8 kg/s. This shows that the maximum temperatures are very dependent on the specific geometry, because the temperatures cannot be lowered to a preset value just by increasing the air mass flow. There is therefore a lower limit on the maximum fuel temperature for a given air inlet temperature and tank geometry.

In Appendix D the results are listed in tabular form in Table 24, and the temperature contour plots of the components are shown in Figure 32 to Figure 35.

## 4.3 Passive Flow without Chimney

The method used to simulate the passive cooling of the tanks is to specify applicable pressure values at the inlet and outlet boundaries. The mass flow is therefore not fixed, and is solved for during the iterative solution process.

The pressure at the inlet and outlet boundaries is specified as the piezometric pressure with a value of 101.3 kPa. The actual static pressure at the boundary is calculated by the code as a function of the piezometric pressure, density and height above the reference point. The zero pressure difference actually means that there is no external force acting on the flow. This approach is very useful, because the static pressure at the boundaries does not have to be calculated for each boundary height.

**Table 9: Results for passive operation without chimney.**

| Case | Filling Level (%) | Mass Flow (kg/s) | Maximum Temperatures | | | | | |
|---|---|---|---|---|---|---|---|---|
| | | | Fuel (°C) | Tank (°C) | Concrete (°C) | Concrete Bottom (°C) | Concrete Top (°C) | Air Outlet (°C) |
| G | 20 | 2.91 | 380.5 | 346.7 | 98.7 | 98.7 | 71.8 | 86.9 |
| H | 100 | 3.30 | 403.1 | 381.6 | 167.8 | 106.8 | 167.8 | 196.8 |

From Table 9 it can be seen that the mass flow reduced from the value specified for the normal operation cases as shown in Table 23 in Appendix C. The resulting mass flow is 2.91 kg/s and 3.3 kg/s for the 20% and 100% filled tanks respectively. The reduced mass flow causes the maximum temperatures of the major components to increase.

The maximum temperature of the fuel increased by 57.4 °C and 70 °C for the two cases when it is compared to the results with forced air flows of 6 kg/s.

The temperature results are shown as contour plots in Figure 36 to Figure 38 in Appendix E.

## 4.4 Effect of Chimney on Passive Cooling Ability

The addition of a chimney should aid the stability of the buoyancy driven flow. The design of the chimney is, however, very important, because an incorrect design can have a negative effect on the flow and resulting temperatures.

The results presented show the effect on the resulting mass flow and maximum temperatures of the components based on the following parameters:

- Chimney cross-sectional area.
- Chimney length.
- Heat transfer at chimney walls.

### 4.4.1 Chimney cross-sectional area

The effect of the area reduction on the maximum temperature of the components and the resulting mass flow is shown in Figure 17. It can be seen that decreasing the area decreases the mass flow, while the maximum temperatures of the fuel and tank increases.

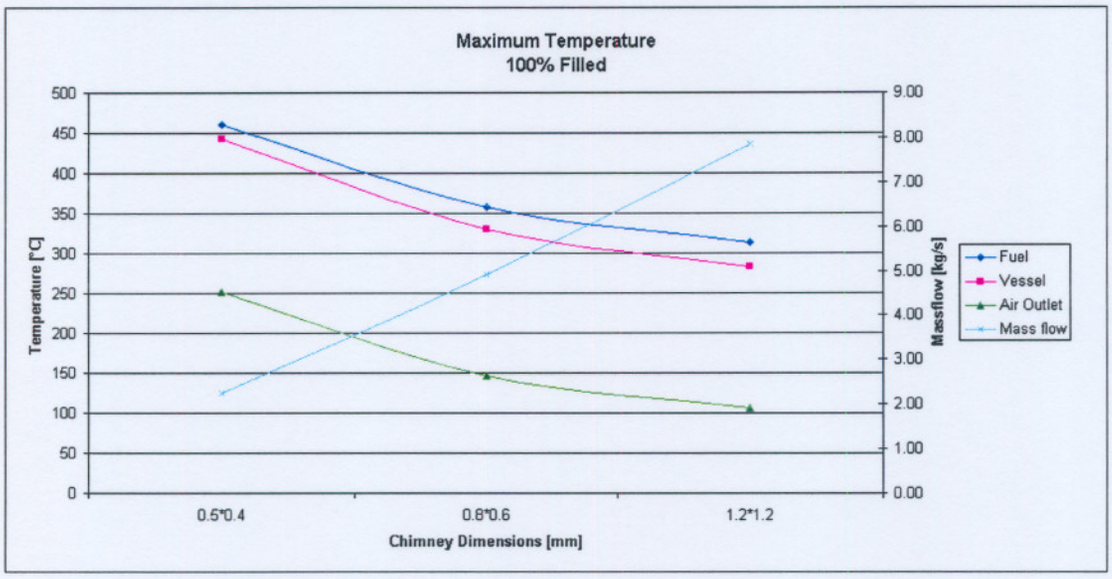


**Figure 17: Effect of chimney cross-sectional area on temperature and mass flow results.**

Reducing the flow area of the chimney reduces the mass flow for two reasons:

- The smaller area results in higher velocities. This increases the total pressure drop over the chimney because the pressure drop is a function of the velocity squared.
- The acceleration of the fluid due to the smaller flow area converts some of the pressure that is required to drive the flow into kinetic energy due to Bernoulli's law. This effect reduces the available pressure to drive the flow due to the higher losses at the exit of the chimney, also as a function of the velocity squared.

The decrease in the pressure over the chimney reduction (0.5 x 0.4) can be seen in Figure 18.

It can be seen from Figure 18 that the pressure drop over the reduction is in the order of 83 Pa for the chimney with an area of 0.5 x 0.4 $m^2$. This is quite a large pressure drop when buoyancy driven flow is concerned. The ideal would be to have no reductions in the chimney, but due to practical sizes and limitations on the area available inside the building, reductions and bends may be required.

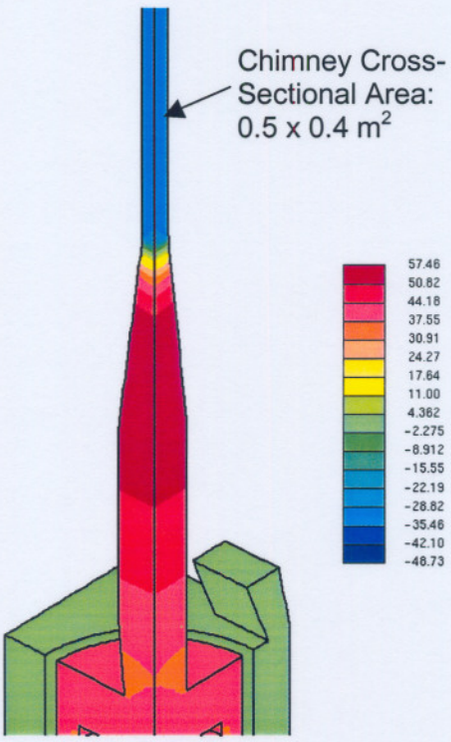


**Figure 18: Piezometric pressure drop (relative) over chimney reduction.**

The pressure contour plots for the rest of the models are given in Figure 39 in Appendix F.

From Figure 17 it is clear that a cross-sectional area of 0.5 x 0.4 $m^2$ is insufficient, because the maximum fuel temperature is above the limit of 400 °C. Of the cases investigated, the chimney with a cross-sectional area of 0.6 x 0.8 $m^2$ is the smallest that results in a maximum fuel temperature below the limit of 400 °C [6].

It is clear from Figure 17 that there is a cross-sectional area between the areas 0.5 x 0.4 and 0.6 x 0.8 that would still give results with a maximum fuel temperature below 400 °C. The area of 0.6 x 0.8 should, however, be considered to be the lower limit until more chimney designs have been investigated.

### 4.4.2 Chimney length

It is expected that a longer chimney would result in an increased mass flow due to the bigger buoyancy force acting on the gas volume. The amount by which it changes is a function of the geometry and the pressure losses within the system.

The effect of the length of the chimney on the mass flow and maximum temperature results for a 20% and 100% filled tank can be seen in Table 10. As expected, the mass flow decreases as the chimney is shortened. The decrease in mass flow is 0.23 kg/s and 0.4 kg/s for the 20% and 100% filled cases respectively.

**Table 10: Effect of chimney length on mass flow and maximum temperatures.**

| Case | Filling Level (%) | Chimney Length (m) | Mass Flow (kg/s) | Maximum Temperatures | | | | | |
|---|---|---|---|---|---|---|---|---|---|
| | | | | Fuel (°C) | Tank (°C) | Concrete (°C) | Concrete Bottom (°C) | Concrete Top (°C) | Air Outlet (°C) |
| K | 20 | 27 | 3.74 | 359.0 | 324.3 | 101.3 | 101.3 | 76.1 | 75.8 |
| M | 20 | 15 | 3.51 | 364.5 | 329.9 | 108.3 | 108.3 | 78.5 | 78.6 |
| L | 100 | 27 | 4.90 | 356.5 | 329.7 | 144.4 | 92.8 | 144.4 | 145.7 |
| N | 100 | 15 | 4.50 | 365.5 | 339.5 | 153.0 | 93.9 | 153.0 | 154.9 |

The effect of the lower mass flow on the temperature results is not that significant. The increase in the maximum fuel temperature is only 5.5 °C and 9 °C for the 20% and 100% filled tanks respectively.

The change in temperature is shown graphically in Figure 40 and Figure 41 in Appendix G. From the figures it can be seen that the relative change in the maximum temperatures is very small.

### 4.4.3 Chimney heat transfer

A hot chimney will transfer heat to the environment. This heat must be taken from the fluid flowing in the chimney. Because the temperature of the gas decreases when heat is removed, the density increases, and the buoyancy force therefore decreases simultaneously. It is therefore expected that the

mass flow through the system is decreased when the chimney is not ideally insulated.

The results presented in Table 11 confirm the above in that the mass flow reduces when there is heat transfer from the chimney walls. The effect on the maximum temperatures is, however, very small, and the variance falls within the convergence error of the models. The maximum fuel temperatures varied by between 1.5 °C and -0.5 °C for the 20% and 100% filled cases respectively.

**Table 11: Effect of chimney heat transfer on mass flow and maximum temperatures.**

| Case | Filling Level (%) | Heat Transfer Coefficient ($W/m^2.K$) | Mass Flow (kg/s) | Maximum Temperatures | | | | | |
|---|---|---|---|---|---|---|---|---|---|
| | | | | Fuel (°C) | Tank (°C) | Concrete (°C) | Concrete Bottom (°C) | Concrete Top (°C) | Air Outlet (°C) |
| K | 20 | 0 | 3.74 | 359.0 | 324.3 | 101.3 | 101.3 | 76.1 | 75.8 |
| O | 20 | 5 | 3.70 | 360.5 | 325.3 | 94.7 | 94.7 | 72.3 | 71.0 |
| L | 100 | 0 | 4.90 | 356.5 | 329.7 | 144.4 | 92.8 | 144.4 | 145.7 |
| P | 100 | 5 | 4.89 | 356.0 | 329.1 | 141.8 | 86.3 | 141.8 | 145.2 |

The heat transfer from the chimney is presented in Table 26 in Appendix H. From the table it can be seen that between 8% and 11.8% of the total heat is lost in the chimney due to the boundary condition applied. As discussed above, the heat lost had a very small effect on the total mass flow and the resulting temperatures.

The change in temperature is shown graphically in Figure 42 and Figure 43 in Appendix H. From the figures it can be seen that the relative changes in the maximum temperatures are very small, and almost negligible.

The heat transfer coefficient chosen is typical for buoyancy driven heat transfer from flat surfaces. The application of the heat transfer coefficient therefore represents the cooling of the outer surface of ducting with a very thin conducting wall. From the results presented, it is evident that the heat transfer from the chimney does not have a significant effect on the mass flow and maximum fuel temperatures.

# CHAPTER FIVE: VERIFICATION

This chapter highlights the strategies implemented to ensure that the results generated with the CFD code are accurate and without any major errors. This includes the processes followed to ensure high-quality input data, the comparison of results with those obtained using another code, and the checks to ensure that the models did converge.

## 5.1 Input Data Integrity

The data used was taken from referenced sources, including the following inputs:

- All boundary conditions specified.
- Material properties.
- Geometrical inputs.

All the above inputs are obtained from configuration-controlled documents, and the data contained in them is controlled according to the PBMR Quality Assurance (QA) processes [25].

The implementation of the data is verified by using checklists to ensure that the data is applied correctly in the CFD code.

## 5.2 Simulation Integrity

The used fuel tank is a complex geometry with very complex heat transfer mechanisms. It is possible to model most of these mechanisms with simplified models, but the effort required to prove that they are applied correctly and within their intended scope may be immense. It was therefore decided to verify the results by making use of another CFD code that has the same capabilities as STAR-CD.

It must be noted that, due to the complexity of the models, differences in code modelling strategies and the vast amount of settings required to set up a CFD model of this nature, it is expected that there will be some differences in the

results. The aim was therefore to make use of similar inputs for the models to the best knowledge of the user. The purpose of the comparison is therefore not to determine the differences in the codes and their capabilities, but to show that similar results can be obtained, irrespective of the choice of code.

### 5.2.1 Use of FLUENT for verification purposes

The PBMR is still in the concept design phase, and for this reason most of the design is done by means of numerical simulation. The reason for this is that experimental work can be very time-consuming and expensive. Due to the size of the equipment being designed, it would often be necessary to scale the geometry to limit the costs of the experiment. This can become a very complex exercise due to the different non-dimensional groups that should be preserved. With the above in mind, it was therefore decided to make use of another CFD code for verification purposes.

STAR-CD has been chosen as the code to do most of the thermo-hydraulic work on the PBMR. FLUENT, on the other hand, is also used at PBMR, and it is widely used in industry. Based on sales figures, these two codes are the leaders in the field of CFD. The two codes are developed independently of each other, and it is therefore believed that they can be used to verify each other's results.

It is accepted that the absolute values calculated with these codes may still be different from actual plant data, but the confidence in the results would be higher if the two codes predict similar results.

The following aspects should be taken into consideration when two CFD codes are used to model the same case:

a. Numerical mesh

   The decision was made to use the same numerical mesh to limit the differences between the two models. This was possible, because the original mesh was created in GAMBIT, the meshing tool of FLUENT.

b. Models

The CFD codes generally offer more than one choice to model a specific process. This includes models such as turbulence, radiation and porous media. The choice of these models will be discussed later in the text.

c. Boundary conditions

The application of boundary conditions should be the same, but the way they are specified may differ between CFD codes. Care should therefore be taken to ensure that the resulting boundary conditions are the same.

d. Solution settings

The solution algorithm of the two codes may differ. In general this should not make a difference to the results, because the solution should converge to the same result if the governing conservation laws are satisfied.

### 5.2.2 Model implementation

As mentioned previously, the models used to compare results obtained with two different codes should be similar. There are differences and similarities in models such as the following, available in STAR-CD and FLUENT:

- Turbulence models.
- Radiation models.
- Porous media model.

The differences and similarities between these two models will be discussed briefly.

a. Turbulence model

FLUENT also has the standard k-ε turbulence model available [14]. This model was used with its default settings.

b. Radiation model

The DTRM model was chosen for use in FLUENT. Like the radiation model in STAR-CD, the DTRM model also groups the surfaces participating in the radiation into clusters (patches in STAR-CD) and then determines the view factors of the various clusters with respect to one another [14].

To calculate the radiation heat transfer between surfaces, it is required to know which surfaces participate in the radiation heat exchange before the view factors of these surfaces can be determined. FLUENT uses the same methodology as STAR-CD to do the above calculation.

The major difference between the two models is that STAR-CD's radiation model allows one to ignore the radiation to the fluid/gas and only calculate radiation heat exchange between surfaces. Radiation to the fluid is therefore an option. In FLUENT, the fluid always takes part in the radiation process, and the volumes are also divided into smaller volumes or clusters to participate in the ray tracing process. The effect of radiation on the fluid can be ignored if the absorption factor is set to a very small number, eliminating the effect of the fluid in the radiation process. The participation of the volume clusters in the ray tracing process can, however, not be ignored, and will always form part of the process. This additional computational load will increase the time required to do the ray tracing.

c. Porosity of bed

The way the porosity is implemented in the two codes is quite different, particularly the specification of boundary conditions for the turbulence models. It was therefore decided to represent the fuel using a solid with an effective thermal conductivity. The pressure in the tank is low (1 ATM), and the buoyancy driven flow would be very small. The representation of a packed bed with effective properties is a common approach in the analysis of pebble bed reactors [26].

It can be seen from Figure 19 that the maximum temperatures compare well, while the minimum temperatures differ substantially. It is believed that the two codes differ in the way they report data on surfaces between materials, and that this is the reason for the difference.

It can be seen that the differences are more pronounced at the upper and lower extremes of the fuel volume.

The differences can be explained by the fact that the cell temperatures are solved during the solution, while the node temperatures are calculated during the post-processing to make plots. During post processing, the data is interpolated from the cell centres to the nodes for the plots shown. It seems as if the post processing interpolation methodology used by the two codes to interpolate data at the interface between different materials differs.

The decision to model the fuel as a solid can be seen when the results presented in Figure 19 are compared to those of the 15% filled case in Figure 22 in Appendix C. The maximum fuel temperatures for the cases where the fuel is modelled as a solid compared to the inclusion of buoyancy are 317.1 C and 316.4 C. The fact that the temperature difference is small cannot be used to argue that the omission of the buoyancy is negligible. The reason this statement cannot be made is due to the fact that the top layer of the fuel is modelled as a solid to facilitate the modelling of radiation from this surface.

**Table 12: Comparative temperature results.**

| Case | Code | Maximum Temperatures (°C)[3] | | | |
|---|---|---|---|---|---|
| | | Fuel | Tank | Concrete | Air Outlet |
| uft-r2-15%-solid | STAR-CD | 318.0 | 267.9 | 70.6 | 56.7 |
| uft-r2-15-ref2 | FLUENT | 309.9 | 259.9 | 67.9 | 56.7 |

This approach limits the natural convection in the fuel, which acts as an

[3] Cell-centred data.

additional heat transfer mechanism. It is believed, however, that this approach is conservative in the sense that less heat is removed from the fuel, resulting in higher fuel temperatures. This approach should be revised once the modelling capabilities of the CFD codes allow thermal radiation from porous media.

The temperature distributions of the tank and concrete are shown in Figure 44 and Figure 45 in Appendix I. These temperature distributions compare quite well with the differences of the maximum temperatures for the tank and the concrete, 4.8 °C and 6.4 °C respectively.

b. Heat transfer between fuel and tank

The heat transfer over selected surfaces is shown in Table 13. It can be seen that there are differences in the values predicted by the two codes. These differences are more pronounced in the inner surfaces of the outer pipes – there is a difference of 7.8%. In general it looks as if the distribution of the heat predicted by the two codes to the different areas is slightly different. The fact that the maximum fuel temperatures are in close agreement indicates that this difference in heat distribution has a small effect on the predicted temperatures.

**Table 13: Surface heat transfer comparison.**

| Description | Boundary Region | STAR-CD | FLUENT |
|---|---|---|---|
| Fuel top surface | 14 | 1 693.0 | 2 397.8 |
| Tank outer surface | 18 | 14 424.0 | 15 029.8 |
| Outer pipes inner surface | 19 | 14 031.0 | 12 938.4 |
| Central pipe inner surface | 20 | 3 894.0 | 3 880.8 |

In general, the results predicted by the two codes compare quite well. There are differences in the results, but the magnitude of the differences is such that the confidence in the results is improved.

Any major modelling errors or misinterpretation of code settings would have been identified if the results did not compare at all.

### 5.2.4 Y-plus values

As mentioned in section 3.6.2, the y-plus values play a very important role in the calculation of convective heat transfer from surfaces during turbulent flow conditions.

A summary of the resulting y-plus values for selected areas is shown in Table 14. The values presented are for the two cases with the highest and lowest y-plus values, and represent the average over the area. These are generally also the two cases with the highest and lowest mass flow rates, because the y-plus value is a function of velocity. The values do not vary much over the surface selected, and the average can be considered a representative value.

**Table 14: Y-plus value summary.**

| Case | Description | Tank Outer Surface | Outer Pipes Inner Surface | Central Pipe Inner Surface |
|---|---|---|---|---|
| F | 20% Filled, 8 kg/s HVAC | 91.12 | 92.16 | 75.81 |
| I | 100% filled, passive flow with small chimney | 29.48 | 37.59 | 33.47 |

From the table it can be seen that most of the values fall in the recommended range of 30 to 100. The lowest value of 29.48 is only marginally below the recommended value of 30, and it is believed that the effect on the results would be negligible. A value smaller than the recommended value would result in an over prediction of the heat transfer coefficient [27].

A summary of all the cases' y-plus values is presented in Table 27 in Appendix J.

## 5.3 Convergence

The convergence of the models is not only based on the default residual reduction, but is also determined by monitoring the convergence of various parameters of interest. The reason this methodology is followed is because the parameters of interest may or may not have converged to the same level as the normalized residuals.

The convergence of the heat fluxes is also a measure of the overall convergence of the model. The convergence of these heat fluxes for one of the models is shown in Figure 20. The heat fluxes shown are typically for the surfaces around the fuel, such as the outer surface of the tank, the pipes' inner surfaces and the top surface of the fuel. It can be seen from the figure that the heat fluxes converged after approximately 5 000 iterations in this instance. For most of the cases, similar convergence was achieved after approximately 5 000 to 8 000 iterations.

## 5.4 Summary

The integrity of simulation results is dictated by a number of factors, such as the inputs used and the convergence of the models. The following methods are used to determine the quality of the results:

- Quality assurance in the input data.
- Comparison of results with another code.
- Convergence checks on various simulation parameters.

Using the above methods and the data presented, it can be assumed that the results presented are of a high quality, and that any major errors would have been picked up during the above process.

It can therefore be concluded that the results presented are fit for use in further design work on the PBMR.

# CHAPTER SIX: CONCLUSION AND RECOMMENDATIONS

## 6.1 Conclusion

The following conclusions can be drawn from the cases investigated:

- With cooling of 6 kg/s, the maximum fuel temperature occurs in the 100% filled tank.
- If the cooling of the 20% filled tank is reduced to 3 kg/s, the maximum fuel temperature stays below the limit of 400 °C at 377.8 °C.
- The temperatures decrease drastically if the cross-sectional area of the chimney is increased.
- The temperature and mass flow results are not very sensitive to the length of the chimney. When the length is reduced from 27 m to 15 m, the maximum fuel temperature increases from 356.5 °C to 365.5 °C, an increase of 9 °C. The mass flow reduced from 4.9 kg/s to 4.5 kg/s, a decrease of 0.4 kg/s.
- From the results presented, it seems as if the mass flow and temperature results are almost unchanged when heat transfer through the chimney wall is considered.
- The results obtained using STAR-CD and those obtained using FLUENT were similar. The difference in the fuel temperature predicted by the two codes is 5.8 °C, although the minimum temperatures differ more. At this stage it is believed that the difference is mainly due to differences in the way in which the results are post-processed.
- The quality of the mesh around the tank is acceptable, based on the y-plus values that are within the allowable range.

## 6.2 Recommendations

The following aspects should be considered for future work:

- Accurate modelling of inlet and outlet geometry to verify the effect on the passive cooling modes.
- Investigate and include the effect of wind direction on the passive cooling ability.
- Include the effect of the other tanks surrounding the used fuel tank. This may be required to validate the assumption of a fixed temperature on the outer surface of the concrete cavity.
- Sensitivity studies on the major input parameters to determine a confidence band. This includes mesh sensitivity studies.

# REFERENCES


[1] PBMR Brochure. 2003. PBMR Document Control Centre. P.O. Box 9396. Centurion. 0046. South Africa.

[2] George, A.P. 2001. Introduction to the Pebble Bed Modular Reactor. Rev. 1. PBMR Document Control Centre. P.O. Box 9396. Centurion. 0046. South Africa.

[3] Modular Milestone. 2003. *Popular Mechanics*. 1(7):85.

[4] Kugeler, K. Alkan, Z. & Pöppe, N. 2003. High temperature reactor technology. Course Notes. Potchefstroomse Universiteit vir Christelike Hoër Onderwys.

[5] Koster, A. 2003. Fundamentals of PBMT safety design. PP000-017556-4705. PBMR Document Control Centre. P.O. Box 9396. Centurion. 0046. South Africa.

[6] Reitsma, F. 2002. Reactor Neutronics – Decay heat for PBMR 400MW design using DIN-25485 standard. MR100-013836-3240. PBMR Document Control Centre. P.O. Box 9396. Centurion. 0046. South Africa.

[7] Willemse, P. 2003. FHSS development specification. MF000-016062-4325. PBMR Document Control Centre. P.O. Box 9396. Centurion. 0046. South Africa.

[8] Fuls, W.F. 2002. A Cost Effective Bulk storage design for the PBMR spent fuel. Potchefstroom: PU vir CHO. (Dissertation – M.Eng.)

[9] Reddy, J.N. 1993. An introduction to the finite element method. McGraw-Hill.

[10] CD Adapco Group. 2001. STAR-CD V3.15. Methodology.

[11] Heng, X., Zujing, G. & Zhiwei, Z. 2002. A numerical investigation of natural convection heat transfer in horizontal spent-fuel storage casks. *Nuclear engineering and design*. 213:59-65.

[12] Stoker, C. 2003. Preliminary UFT design criticality calculations. MF000-017461-3480 Rev. 1. PBMR Document Control Centre. P.O. Box 9396. Centurion. 0046. South Africa.

[13] Fuls, W.F. 2002. Used Fuel Tank CFD Input Variables. FH-A-000000-132 Rev. A. PBMR Document Control Centre. P.O. Box 9396. Centurion. 0046. South Africa.

[14] Fluent Inc. 2003. Fluent 6.1 User's Guide.

[15] VDI Wärmeatlas, Wärmeleitfahigkeit von Schüttschichten, 6. Auflage 1991.

[16] Coetzee, S. 2001. A CFD evaluation investigating the effect of thermal radiation from the fuel spheres to the inner tank walls. 00353/055. PBMR Document Control Centre. P.O. Box 9396. Centurion. 0046. South Africa.

[17] Jansen van Rensburg, P.A. 2001. PBMR Thermo physical properties. 003392-34/1. PBMR Document Control Centre. P.O. Box 9396. Centurion. 0046. South Africa.

[18] CD Adapco Group. 2001. STAR-CD V3.15, PROSTAR Commands.

[19] White, F.M. 1991. Viscous fluid flow. 2nd ed. McGraw-Hill.

[20] Ramesh, N. & Merzkirch, W. 2001. Combined convective and radiative heat transfer in side-vented open cavities. *International Journal of Heat and Fluid Flow*. 22:180-187.

[21] Viljoen, C.F. 2002. A CFD evaluation of the Used Fuel Tank with and without forced cooling. 011242/A. PBMR Document Control Centre. P.O. Box 9396. Centurion. 0046. South Africa.

[22] Incropera F.P. & De Witt, D.P. 1996. Fundamentals of mass and heat transfer, 4th ed. USA : John Wiley & Sons.

[23] Kim, S. Kim, M.C. 2002. A scale analysis of turbulent heat transfer driven by buoyancy in a porous layer with homogeneous heat sources. *Int. Comm. Heat Mass Transfer.* 29(1):127-134.

[24] Van Staden, M.P. 2001. PBMR Core Structures – Phase 3A Thermo-Hydraulic Report. 009905-313/A. PBMR Document Control Centre. P.O. Box 9396. Centurion. 0046. South Africa.

[25] Wimpey, D.G. 2001. Control of design input, QAP_0402N. PBMR Document Control Centre. P.O. Box 9396. Centurion. 0046. South Africa.

[26] International Atomic Energy Agency. 2001. Heat transport and afterheat removal for gas cooled reactors under accident conditions. IAEA, Wagramer Strasse 5, P.O.Box 100, A-1400 Vienna, Austria.

[27] Adapco online, Heat Transfer Coefficients, Their meaning and use. (http://www.adapco-online.com/feature_arts/htc/htran.html). 3 March 2003.

[28] EUROPEAN RESEARCH COMMUNITY ON FLOW, TURBULENCE AND COMBUSTION. 2000. ERCOFTAC Special Interest Group on 'Quality and Trust in Industrial CFD'. Best Practice Guidelines.

[29] Rousseau, P.G. 2000. Equations and input parameters for the PBMR pebble bed reactor simulations model. PBMR-0001 Rev. 2. PBMR Document Control Centre. P.O. Box 9396. Centurion. 0046. South Africa.

# APPENDIX A.: MATERIAL PROPERTIES

**Table 15: Material properties of air.**

| Property | Value | Unit |
|---|---|---|
| | $TS = \frac{T}{273.15}$ | |
| Density | $R = 287$<br>$Z = 1$<br>$\rho = \frac{P}{Z \cdot R \cdot T}$ | $kg/m^3$ |
| Viscosity | $\mu = 1E-7 * \left(186.0507215 * 0.9148561237^{TS} * TS^{0.8835914154}\right)$ | kg/m.s |
| Conductivity | $k = 0.0271384778 * 0.8906898514^{TS} * TS^{1.01478317}$ | W/m.K |
| Specific heat | $c_p = 921.3071033 * 1.091808211^{TS} * TS^{-0.0786761672}$ | J/kg.K |

**Table 16: Material properties of helium.**

| Property | Value | Unit |
|---|---|---|
| Density | $R = 2077.27$<br>$Z = 1 + 0.4446E-5 * \frac{P}{T^{1.2}}$<br>$\rho = \frac{P}{Z \cdot R \cdot T}$ | $kg/m^3$ |
| Viscosity | $\mu = 3.674E-7 * T^{0.7}$ | kg/m.s |
| Conductivity | $k = 2.682E-3 * T^{0.71*(1-2E-9*P)} * (1+1.123E-8*P)$ | W/m.K |
| Specific heat | $c_p = 5195$ | J/kg.K |

**Table 17: Material properties of fuel.**

| Property | Value | Unit |
|---|---|---|
| Density | $R = 2077.27$<br>$Z = 1 + 0.4446E-5 * \frac{P}{T^{1.2}}$<br>$\rho = \frac{P}{Z \cdot R \cdot T}$ | $kg/m^3$ |
| Viscosity | $\mu = 3.674E-7 * T^{0.7}$ | kg/m.s |
| Conductivity | $k_{eff} = 1.2673E-4 * T^{1.6433}$ | W/m.K |
| Specific heat | $c_p = 5195$ | J/kg.K |

**Table 18: Material properties of tank.**

| Property | Value | Unit |
|---|---|---|
| Conductivity | $k = 45$ | W/m.K |

**Table 19: Material properties of concrete.**

| Property | Value | Unit |
|---|---|---|
| Conductivity | $k = 2.41$<br>if $0 < T < 65$ °C<br>$k = 9.1483 * (T-273)^{-0.3195}$<br>if 65 °C > $T$ > 500 °C | W/m.K |

**Table 20: Material properties of shield.**

| Property | Value | Unit |
|---|---|---|
| Conductivity | $k = 0.064$ | W/m.K |

**Table 21: Material properties of gamma shield.**

| Property | Value | Unit |
|---|---|---|
| Conductivity | $k = 35$ | W/m.K |

# APPENDIX B.: CALCULATIONS

## B.1 Temperature Gradient in Pebble during Decay Heat

The temperature gradient in the spherical fuel element during steady state conditions can be calculated from [22]:

$$\frac{1}{r^2}\frac{\partial}{\partial r}\left(r^2 \cdot k \cdot \frac{\partial T}{\partial r}\right) + q''' = 0 \qquad \text{[A-1]}$$

By keeping k and q''' constant, evaluation of the differential equation to calculate the temperature gradient across the fuel element gives:

$$\Delta T = \frac{q''' \cdot r_0^{\,2}}{6 \cdot k} \qquad \text{[A-2]}$$

As a first order calculation, assume the heat generation is spread evenly over the entire pebble.

| Variable | Value | Unit | Comments |
|---|---|---|---|
| $r_0$ | 0.03 | m | Outer radius of pebble. |
| q''' | 11030 | $W/m^3$ | Decay heat at time at t=10d. (Start of defuelling.) |
| k | 33 | W/m.K | Volume average thermal conductivity [29]. |
| ε | 0.39 | | Porosity [29]. |

The heat generation given is based on the volume of the pebble and the voids between them. To get the heat generated in a pebble, it is necessary to divide by the porosity:

$$\begin{aligned} q'''_{pebble} &= q'''/(1-\varepsilon) \\ &= 11030/(1-0.39) \\ &= 18082 \end{aligned} \qquad \text{[A-3]}$$

The temperature difference is then calculated as:

$$\Delta T = \frac{q'''_{pebble} \cdot r_0^2}{6 \cdot k}$$
$$= \frac{18082 \cdot 0.03^2}{6 \cdot 33} \qquad [A\text{-}4]$$
$$= 0.072°C$$

The low temperature gradient within the pebble gives confidence in the approach of not modelling the heat transfer in the pebble.

## B.2 Calculation of Effective Conductivity of Thermal Shield

The shield is sufficiently thin ($\Delta x << r$) to assume that the heat transfer through the shield can be solved using standard heat transfer equations in a Cartesian coordinate system:

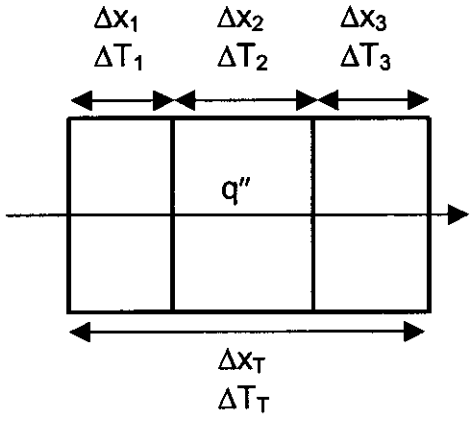


**Figure 21: Calculation of effective conductivity.**

The heat transfer through the entire assembly can be calculated with [22]:

$$q'' = \frac{\Delta T_T}{R_T}, \ [W/m^2] \qquad [A\text{-}5]$$

where:

$$R_T = \frac{\Delta x_T}{k_T} \qquad [A\text{-}6]$$

The heat transfer through each of the sections is equal and can be calculated as:

$$q'' = \frac{\Delta T_1}{R_1} = \frac{\Delta T_2}{R_2} = \frac{\Delta T_3}{R_3} \qquad [A\text{-}7]$$

The total temperature difference is the sum of all the differences giving:

$$\Delta T_T = \Delta T_1 + \Delta T_2 + \Delta T_3 \qquad [A\text{-}8]$$

From [A-6], [A-7] and [A-8] it can be shown that the total resistance is the sum of all the resistances, giving:

$$\frac{\Delta x_T}{k_T} = \frac{\Delta x_1}{k_1} + \frac{\Delta x_2}{k_2} + \frac{\Delta x_3}{k_3} \qquad [A\text{-}9]$$

or written in terms of $k_T$:

$$k_T = \frac{\Delta x_T}{\frac{\Delta x_1}{k_1} + \frac{\Delta x_2}{k_2} + \frac{\Delta x_3}{k_3}} = \frac{\Delta x_T}{R_T} \qquad [A\text{-}10]$$

The calculated results are presented in Table 22.

**Table 22: Calculation of effective conductivity of thermal shield.**

| Material | Carbon Steel | Insulation | Aluminium Foil | Total |
|---|---|---|---|---|
| Δx [m] | 0.001 | 0.01 | 0.0001 | **0.0111** |
| k [W/m.K] | 40 | 0.058 | 174 | |
| R (=Δx/k) [W/K] | 2.5E-5 | 0.172 | 5.75E-07 | **0.1724** |
| | | | **$k_T = \Delta x_T / R_T$** | **0.06437** |

# APPENDIX C.: EFFECT OF FILLING LEVEL ON RESULTS

**Table 23: Effect of filling level on maximum temperatures.**

| Case | Filling Level | Maximum Temperatures (°C) | | | | | |
|---|---|---|---|---|---|---|---|
| | | Fuel | Tank | Concrete | Concrete Bottom | Concrete Top | Air Outlet |
| A | 10 | 295.4 | 240.6 | 86.2 | 86.2 | 49.6 | 50.5 |
| B | 15 | 316.4 | 266.6 | 76.3 | 76.3 | 55.2 | 56.7 |
| C | 20 | 323.1 | 282.1 | 74.8 | 74.8 | 60.6 | 63.0 |
| D | 100 | 333.1 | 304.7 | 122.4 | 71.3 | 122.4 | 128.2 |